

CHORUS

This is the accepted manuscript made available via CHORUS. The article has been published as:

Structure and properties of Fe-modified  
 $\text{Na}_{\{0.5\}}\text{Bi}_{\{0.5\}}\text{TiO}_{\{3\}}$  at ambient and elevated  
temperature

Elena Aksel, Jennifer S. Forrester, Benjamin Kowalski, Marco Deluca, Dragan Damjanovic,  
and Jacob L. Jones

Phys. Rev. B **85**, 024121 — Published 30 January 2012

DOI: [10.1103/PhysRevB.85.024121](https://doi.org/10.1103/PhysRevB.85.024121)

## Structure and properties of Fe-modified $\text{Na}_{0.5}\text{Bi}_{0.5}\text{TiO}_3$ at ambient and elevated temperature

Elena Aksel<sup>1</sup>, Jennifer Forrester<sup>1</sup>, Benjamin Kowalski<sup>1</sup>, Marco Deluca<sup>2,3</sup>, Dragan Damjanovic<sup>4</sup> and Jacob L. Jones<sup>1</sup>

<sup>1</sup>*Department of Materials Science and Engineering, University of Florida, Gainesville, FL 32611, USA*

<sup>2</sup>*Institut für Struktur- und Funktionskeramik, Montanuniversität Leoben, A-8700 Leoben, Austria*

<sup>3</sup>*Materials Center Leoben Forschung GmbH, A-8700 Leoben, Austria*

<sup>4</sup>*Ceramics Laboratory, Swiss Federal Institute of Technology (EPFL), Lausanne 1015, Switzerland*

### Abstract

Sodium bismuth titanate (NBT) ceramics are among the most promising lead-free materials for piezoelectric applications. This work reports the crystal structure and phase evolution of NBT and Fe-modified NBT (from 0-2 at% Fe) using synchrotron X-ray diffraction and Raman spectroscopy, both at ambient and elevated temperatures. The crystallographic results are discussed with reference to permittivity and piezoelectric thermal depolarization measurements of the same compositions. Changes in the depolarization temperature due to Fe substitution were detected by Raman spectroscopy, and were found to correlate closely with depolarization temperatures obtained from converse piezoelectric coefficient and permittivity measured *in situ*. The depolarization temperatures obtained from direct piezoelectric coefficient measured *ex situ* as well as the phase transition temperatures obtained from synchrotron X-ray diffraction were found to be at higher temperatures. The mechanisms underlying the relationship between permittivity and piezoelectric depolarization to structural transitions observed in Raman spectroscopy and X-ray diffraction are discussed.

## I. Introduction

$\text{Na}_{0.5}\text{Bi}_{0.5}\text{TiO}_3$  (NBT) has recently received considerable attention as a potential replacement for the commonly used Lead (Pb)-based piezoelectric material, lead zirconate titanate (PZT). NBT was first reported in the 1960s by Smolenskii *et al.*<sup>1</sup> and has historically been described as exhibiting the rhombohedral  $R3c$  space group at room temperature.<sup>2</sup> There has been some recent debate over the structure of NBT, especially concerning the nature of the structural transitions with changing temperature.<sup>2-5</sup> The transitions in NBT with temperature were re-examined by Dorcet *et al.* using transmission electron microscopy, with the conclusion that the transition from the room temperature rhombohedral phase to the high temperature tetragonal phase occurs through an intermediate modulated phase consisting of orthorhombic ( $Pnma$ ) platelets in rhombohedral ( $R3c$ ) perovskite blocks.<sup>4</sup> Recent single crystal neutron diffraction experiments by Gorfman and Thomas<sup>6</sup>, and high resolution X-ray powder diffraction studies of polycrystalline materials by Aksel *et al.*<sup>7</sup> have provided new insight into the crystallographic structure of NBT. Refinement of the diffraction patterns through the Rietveld method in both cases has indicated a room temperature average structure in the  $Cc$  space group rather than  $R3c$ .<sup>6, 7</sup> In addition, Dorcet *et al.*<sup>8</sup> as well as Beanland and Thomas<sup>9</sup> observed inclusions of tetragonal  $P4bm$  platelets in this material at room temperature.

Although the Curie temperature,  $T_c$ , of NBT is reported to be at 320 °C,<sup>1</sup> the piezoelectric properties of this material diminish at a much lower temperature (Fig. 1). This piezoelectric depolarization temperature,  $T_d$ , was reported by Hiruma *et al.* as 187 °C and it is strongly affected by the Na/Bi stoichiometry.<sup>10</sup> However, structural studies of NBT using neutron diffraction did not report any structural transitions near the temperature range of the  $T_d$ .<sup>2</sup> In their TEM studies, Dorcet *et al.* reported the formation of  $Pnma$  platelet shaped domains at 200 °C.<sup>4</sup> Recent work from Aksel *et al.* presented *in situ* high resolution X-ray

diffraction measurements of NBT during heating and attributed the depolarization process to an increase in volume fraction of material which is only present at a short range.<sup>11</sup>

The  $T_d$  of NBT may be modified through the addition of dopants or through the use of solid solution alloying with other perovskite structures. For example, Watanabe *et al.* presented the impact of several lanthanide dopants substituted on the perovskite A-site of NBT and found that the  $T_d$  of NBT decreased with increased dopant content.<sup>12</sup> Davies *et al.* showed an increase in the  $T_d$  with substitution of Fe or Mn on the perovskite B-site.<sup>13</sup> These dopants also increased the piezoelectric coefficient at higher temperatures prior to piezoelectric depolarization.<sup>13</sup> In the case of solid solutions with barium titanate BaTiO<sub>3</sub> (BT), Hiruma *et al.* showed that  $T_d$  decreased with addition of BT up to 6%, which is the proposed morphotropic phase boundary between NBT and BT, and then increased with further addition.<sup>14</sup>

In the NBT-BT system it was shown by Raman spectroscopy that the  $T_d$  is characterized by a loss of long-range ferroelectric order (which is maintained on the short range), rather than being a structural phase transition.<sup>15</sup> The first-order Raman signal, originating from the center of the Brillouin zone, probes coherent scattering on the nanometer length scale and is thus sensitive to short-range order in a crystal lattice. In relaxor or morphotropic ferroelectrics with short-range phase segregation, Raman signals from second phases of nanometer scale but with the same correlation length are superimposed on the overall signal belonging to a macroscopic matrix phase.<sup>16-19</sup> Raman spectroscopy has been used to study phase transitions and the nanoscale structural characteristics of NBT and its solid solutions.<sup>15, 20-24</sup> Due to challenges of intrinsic broadening and overlapping of phonon modes in the assignment of mode symmetries, structural analysis thus relies on analyzing soft-mode or hard-mode behavior as a function of composition, pressure or temperature.<sup>15, 21-</sup>

<sup>24</sup> Other studies in NBT-BT<sup>25</sup> and NBT-SrTiO<sub>3</sub><sup>24</sup> generally confirmed that transitions

involving the ferroelectric behavior are related to subtle local structural distortions and phase coexistence.

In the present work, the long and short range structures in NBT and Fe-modified NBT are examined by Raman spectroscopy and X-ray diffraction (XRD) with the aim of understanding the effect of Fe modification on  $T_d$ . In PZT, Fe substitution is referred to as acceptor doping due to the aliovalent substitution of  $\text{Fe}^{3+}$  ions for the  $\text{Zr}^{4+}$  and  $\text{Ti}^{4+}$  B-site ions.<sup>26</sup> Extensive studies have shown that chemical modification of Ti-based perovskite ferroelectrics with Fe generally leads to so-called material “hardening” characterized by a decrease in the permittivity and piezoelectric coupling factor as well as an increase in the mechanical and electrical quality factor.<sup>26, 27</sup> Some effects of Fe modification in NBT are known. For example, Nagata and Takenaka reported that the addition of Fe to NBT leads to a slight decrease in the  $T_c$ , resistivity, and planar coupling factor as well as an increase in the coercive field,<sup>28</sup> consistent with Fe modified PZT. Davies *et al.* also examined Fe doping in NBT and found that the addition of Fe leads to an increase in  $T_d$  and a decrease in the room temperature piezoelectric coefficient.<sup>13</sup> Even when  $\text{Fe}_2\text{O}_3$  is used as a sintering aid (0.15 at% Fe decreased the sintering temperature to 850 °C),<sup>29</sup> there is a possibility that Fe can incorporate into the lattice and affect properties.

## II. Experimental

Samples were prepared using solid state synthesis as described in Davies *et al.*<sup>13</sup> with  $\text{Fe}_2\text{O}_3$  to obtain concentrations of 0, 0.5, 1.0, 1.5, and 2.0 at% Fe. The addition of  $\text{Fe}_2\text{O}_3$  to the samples was compensated by an appropriate reduction in  $\text{TiO}_2$ . Pellets used for X-ray diffraction (XRD) were crushed into fine powder using a mortar and pestle, and annealed at 400 °C for 3 h in a closed alumina crucible to reduce intra-granular residual stresses. Gold electrodes were sputter deposited onto the major faces of all samples followed by electrical

poling at 4 kV/mm for 5 min in a silicone oil bath held at 80 °C. The electric field was removed from the samples while they were held in the 80 °C oil bath. The samples were set aside for approximately 24 h, after which the direct longitudinal piezoelectric coefficient was measured using a Berlincourt  $d_{33}$  meter (APC Ceramics, Mackeyville, PA). Samples were heated from 25 °C to 550 °C using a heating rate of 2 °C/min while permittivity and loss were measured at five different frequencies: 100 Hz, 1 kHz, 10 kHz, 100 kHz, and 1 MHz, using a precision LCR meter (Hewlett Packard).

High-resolution XRD patterns were measured on beamline 11-BM of the Advanced Photon Source at Argonne National Laboratory. For room temperature measurements, the powders were loosely packed in 0.8 mm diameter polyimide tubes and rotated at 60 Hz during data collection to improve crystallite averaging. Diffraction patterns were measured using a monochromatic X-ray beam with a wavelength of 0.413629 Å and a  $2\theta$  range of 3°-27° with a 0.001° step size in  $2\theta$ . For high temperature measurements, powders were packed into 0.3 mm diameter quartz capillaries, also spun at 60 Hz. Samples were heated from room temperature to 600 °C at a rate of 5 °C/min while XRD patterns were measured. Each pattern was measured for 1.25 min with a step size of 0.002°  $2\theta$ . Longer times of 50 min were then used to measure diffraction patterns at distinct temperatures of 600 °C, 400 °C, 300 °C, 250 °C, and 100 °C. A cooling rate of 5 °C/min was used between these temperatures.

Crystal structure refinements of the powders at room and elevated temperatures were carried out using the Rietveld analysis program General Structure Analysis System.<sup>30</sup> The peak asymmetry increased with higher Fe content, and profile function 4 (with Stephens asymmetry<sup>31</sup>) yielded the closest fit. The peaks generally became more symmetrical during heating, which allowed the use of a combination of profile functions 3 and 4. A single peak fitting procedure was also used to examine the evolution of several selected diffraction peaks as a function of temperature. A polynomial function was used to model the background of the

entire diffraction pattern. An asymmetric Pearson VII-type profile shape function (see Ref. <sup>32</sup>) was also used to fit individual Bragg peaks by employing a least squares algorithm in the program MATLAB (The Mathworks Inc., ver. 7.3.0.267).

Raman spectra were obtained with a LabRAM microprobe system (ISA/Jobin-Yvon/Horiba, Villeneuve d'Ascq, France) using a 532.02 nm Nd:YAG solid state laser as the excitation source. Surfaces of unpoled sintered pellets were prepared by polishing down to a 1  $\mu\text{m}$  diamond paste. The laser light was focused on the sample surface by means of a long working distance and 100x (N.A.=0.8) objective lens (LMPlan FI, Olympus, Japan), allowing the laser beam spot width to be  $\sim 1 \mu\text{m}$  on the investigated position. Effective power at the sample surface was set to 3 mW. Spectra were collected in a true backscattering geometry with the aid of a Peltier-cooled charged coupled device camera allowing a spectral resolution of  $1.5 \pm 0.1 \text{ cm}^{-1}/\text{pixel}$  for the investigated range. Temperature-dependent (*in situ*) Raman experiments were performed in the range 25-255  $^{\circ}\text{C}$  (step: 10  $^{\circ}\text{C}$ ) by means of a Linkam MDS600 heating-cooling stage (Linkam, Tadworth, UK). Temperature accuracy of the stage was checked by means of  $\text{CO}_2$  and  $\text{H}_2\text{O}$  inclusions in transparent minerals. Due to sample expansion with increasing temperature, spectra were collected on different areas of the sample, which required re-focusing at each temperature interval. The measured spectra were deconvoluted and analyzed with commercial software (PeakFit, Systat Software Inc., San Jose, CA) using multiple Gaussian-Lorentzian peak functions.

### III. Results

#### A. Temperature dependence of properties

Measurement of the longitudinal piezoelectric coefficient,  $d_{33}$ , as a function of temperature both *in situ* (converse) and *ex situ* (direct), was reported previously in Davies *et al.*<sup>13</sup> and is reproduced in Fig. 1. Both types of measurements show that the addition of a low

Fe concentration (i.e., 0.5 at%) leads to an increase in the  $T_d$  without a reduction in the room temperature  $d_{33}$ . At 1 at% Fe, the  $T_d$  remains as high as in the 0.5 at% Fe sample, but a decrease in the room temperature  $d_{33}$  is observed. Further increase in Fe content leads to a reduction in both the room temperature  $d_{33}$  and the  $T_d$ . A summary of the measured depolarization temperatures (determined in Ref. <sup>13</sup>) is given in Table I.

Permittivity and loss tangent were also measured as a function of temperature for poled and unpoled samples of the same compositions. Figure 2 shows the permittivity and loss tangent measured at five different frequencies for unmodified and 0.5 at% Fe modified NBT. A large increase in apparent permittivity and loss with temperature is observed in the 0.5 at% Fe sample for low frequencies (Fig. 2(c), (d)) and is likely due to conductivity. Permittivity and loss of samples with a higher Fe content are not shown due to the strong contributions from conductivity. A peak in the loss tangent vs. temperature plot and an inflection point in the permittivity vs. temperature plot are observed around the  $T_d$  for the poled samples. Frequency dispersion is observed in all measured compositions and poling states, consistent with relaxor-type behavior.<sup>33,34</sup> The peak in the loss tangent vs. temperature plot is at 176 °C for unmodified NBT and at 202 °C for 0.5 at% Fe modified NBT (Table I). It is interesting to note that while a distinct peak appears in the loss tangent vs. temperature plot at the  $T_d$  for both poled samples (Fig. 2(a) and (c)), it is more subtle for unpoled samples (Fig. 2(b) and (d)). A slight change in the rate of this transition is also apparent after a small addition of Fe. A sharper increase in permittivity at the  $T_d$  is observed in the 0.5 at% Fe (Fig. 2(c)) sample than in the unmodified one (Fig. 2(a)). This behavior is mirrored in the *in situ* depolarization measurements (Fig. 1(a)), in which the depolarization of the 0.5 and 1.0 at% Fe samples occurs in a narrower temperature range than the unmodified sample.

## B. Crystallographic structure of unmodified and Fe-modified NBT by XRD

Figure 3 shows the evolution of the Bragg peaks with Fe modification, as observed in synchrotron diffraction patterns. The indexed peaks are labeled relative to the pseudo-cubic unit cell. To extract structural information, the diffraction patterns were analyzed using the Rietveld method. All room temperature data were modeled using the  $Cc$  space group, previously presented by Gorfman and Thomas for single crystals<sup>6</sup> and applied to powders of unmodified NBT by Aksel *et al.*<sup>7</sup> A sample refinement of the 1 at% Fe sample is shown in Fig. 4. The fit of the  $Cc$  model used in this refinement shows that there are no second phases present in this composition. This is evidenced by the hkl markers (shown below the pattern in Fig. 4) fully accounting for the peaks in the diffraction pattern. A close examination of the individual diffraction peaks supports the previous finding in Aksel *et al.*<sup>7</sup> that the rhombohedral  $R3c$  structure cannot fully account for the splitting in the peaks.

Changes in the unit cell as well as the criteria of fit are given in Table II. A comprehensive summary of the refinement results for the various Fe modified samples is available in the Supplemental Material at [URL will be inserted by publisher] in Table S.1. With increasing Fe concentration, the  $a$  and  $c$  lattice parameters and monoclinic angle ( $\beta$ ) increase while the  $b$  lattice parameter generally remains constant, indicating that no phase transitions occur. The increase in the lattice parameters and monoclinic angle indicates that the structure distorts further from the prototypical cubic structure with increasing Fe content. Although the oxygen positions are refined in this analysis, they are too variable for an octahedral tilting calculation, due to the insensitivity of X-rays to oxygen. It is possible, however, to infer from the increasing ferroelastic distortion with the addition of Fe that the octahedral tilting increases with Fe substitution. Extra peaks in the XRD pattern of the 2% Fe-modified sample, such as the one at a  $2\theta$  position of  $10.5^\circ$  (Fig. 3), suggest that a secondary phase is present. Indexing the extra peaks revealed that the secondary phase took the perovskite structure, and one possibility is  $\text{BiFeO}_3$  (BFO). Adding the starting model<sup>35</sup> of

BFO as a second phase provided a good fit to the XRD pattern, as seen in the criteria of fit values in Table II.

To determine the preferred perovskite lattice site for Fe substitution, refinements were attempted where Fe occupied the A-site with Na/Bi, although this model led to an unstable refinement. As expected, substitution of Fe on the B-site resulted in a stable refinement, consistent with the substitution scheme in PZT. **An attempt was also made to quantify the occupancies of Fe and Ti on the B-site. For this determination, the starting values for the occupancies were set to the expected values based on the nominal stoichiometry (e.g. for the 1% Fe sample the occupancy of Ti was set to 0.99 and Fe to 0.01). The refinement did not significantly change the starting values. Manual adjustment of the starting values also did not affect the quality of fit. Thus, it was inferred that this method is not sufficiently sensitive to discern the exact Fe occupancy on the B-site, most likely because Fe and Ti have similar X-ray atomic scattering factors.**

Structural analysis was also carried out on the XRD patterns of a 1 at% Fe sample as a function of temperature. A compilation of the patterns is presented in Fig. 5. Each pattern was modeled via the Rietveld method, with a selection of the refined structural information given in Table III. **The full refinement results are presented in Table S.2 of the Supplemental Material at [URL will be inserted by publisher].** These indicate that the evolution of the structure follows a transition from monoclinic  $Cc$  to tetragonal  $P4bm$  and finally to cubic  $Pm\bar{3}m$ , with the tetragonal and cubic phases consistent with previous work from Jones and Thomas.<sup>2</sup> At 250 °C it was found that the  $Cc$  space group could no longer adequately model the pattern. Several phase combinations were trialed, such as  $Cc+R3c$ ,  $Cc+P4bm$ ,  $Cc+Pm\bar{3}m$ , and  $R3c+Pm\bar{3}m$ . The phase combination of  $Cc+Pm\bar{3}m$  provided the closest fit to several aspects of the pattern, including the asymmetry and decreased intensity of the  $\{3/2\ 1/2\ 1/2\}$  reflection and the peak splitting present in the  $\{110\}$  and  $\{111\}$  peaks. The addition

of the  $Pm\bar{3}m$  space group is used to describe local disorder in the average structure which can create small variations in the diffraction patterns that cannot be entirely modeled using a single phase  $Cc$  structure.

While the information presented in Fig. 5 and Table III is given at discrete temperatures, an additional measurement was undertaken where XRD data of unmodified and 1 at% Fe modified NBT was measured continuously as a function of temperature up to 600 °C. Figure 6 shows the evolution of several of the perovskite peaks of NBT (Fig. 6(a)) and 1% Fe-modified NBT (Fig. 6(b)) from room temperature to 600 °C. Structural transitions in the material are apparent through the observed changes in the peak splitting. For example, the {200} peak splitting into two peaks above approximately 285°C for unmodified NBT correlates with a phase transition to tetragonal  $P4bm$ . To examine the presence of structural transitions around the depolarization temperature, the splitting in the 110 peak was evaluated using a single peak fitting procedure with three asymmetric Pearson-VII peak profiles. Based on this fit, a phase transition temperature is estimated when two of the component peaks are indistinguishable within the error of each other. This is observed at 195 °C for unmodified NBT and 220 °C for 1% Fe-modified NBT. The average error associated with these temperatures, based on a 5 °C/min heating rate, is +/- 9 °C. These results are qualitatively consistent with the changes observed in Figure 6.

### C. Raman spectroscopy of unmodified and Fe-modified NBT

A representative Raman spectrum of unmodified NBT and its deconvolution is displayed in Fig. 7(a). The spectrum is consistent with previous reports,<sup>15, 21-24</sup> where it was assigned as belonging to the pseudo-rhombohedral  $R3c$  phase, for which a total of 13 Raman-active modes ( $\Gamma_{\text{Raman}, R3c} = 4A_1 + 9E$ ) are expected.<sup>23</sup> Three main regions can be discerned. The first one at  $\sim 270 \text{ cm}^{-1}$  is dominated by an  $A_1$  mode assigned to Ti-O vibrations. The mid-

frequency region at around 450-700  $\text{cm}^{-1}$  hosts modes associated with the vibration of the  $\text{TiO}_6$  octahedra, most likely as a superposition of transverse optical (TO) and longitudinal optical (LO) bands of  $A_1$  character. The high-frequency region above 700  $\text{cm}^{-1}$  has been linked to  $A_1(\text{LO})$  and  $E(\text{LO})$  overlapping bands.<sup>24</sup>

The Raman spectra of unmodified and modified NBT at room temperature are displayed in Fig. 7(b). Figure 7(c) shows the Raman spectra of unmodified NBT as a function of increasing temperature. The temperature-dependent spectra for the other compositions exhibit similar behavior as observed in the unmodified NBT. The intensities of all represented spectra were corrected for the Bose-Einstein temperature factor. No consistent variation in the peak positions was measured with increasing Fe substitution at room temperature, which is compatible with the small difference in atomic mass on the B-site upon Fe substitution. This is in accordance with observations from XRD (*cf.* section III.B.) and with the fact that Raman spectra are generally only slightly affected for such small concentrations of modifiers. No contribution from a secondary phase of BFO is observed in the measured spectrum of the 2 at% Fe composition most likely because of the proximity of the Raman-active modes of BFO to those of the NBT primary phase.<sup>36</sup>

With increasing temperature, temperature-induced broadening occurs, which in the case of NBT could also support the idea that higher structural disorder exists in the Ti-O bond of the  $\text{TiO}_6$  octahedra with increasing temperature; such behaviour may be associated with the nucleation of nanodomains within the ferroelectric matrix. This was suggested in previous works.<sup>15, 17, 33</sup> In particular, the loss of long-range ferroelectricity at  $T_d$  was proposed to be related to the nucleation of antiparallel nanodomains with tetragonal  $P4bm$  structure.<sup>15, 33</sup> The onset of a secondary phase within the primary one will surely influence the strength of the Ti-O bond, and should thus be visible by examining the softening of the  $A_1$  mode at  $\sim 270$   $\text{cm}^{-1}$  upon increasing temperature. The temperature dependence of this mode for all

compositions is represented in Fig. 8. The displayed results are the average of three experimental runs, on the basis of which the standard deviation is represented as an error bar. The experimental error is contributed by minor differences in characteristics (e.g., local density fluctuations and microscopic residual stress) between each probed position in the sample. An overall softening of the phonon line center is detected over the investigated temperature range, and **most compositions present** an anomaly in the neighborhood of the expected  $T_d$  value obtained from the piezoelectric depolarization measurements (*cf.* Table I). Peak softening with temperature is observed due to anharmonic terms in the vibrational potential energy.<sup>37</sup> This can be generally described by the following equation, taking into account terms of up to four phonons:

$$\omega(T) = \omega_0 + A \left[ 1 + \frac{2}{e^x - 1} \right] + B \left[ 1 + \frac{3}{e^y - 1} + \frac{3}{(e^y - 1)^2} \right] \quad \text{Eq. (1)}$$

where  $x = \hbar\omega_0/2kT$ ,  $y = \hbar\omega_0/3kT$ , with  $k$  the Boltzmann's constant and  $\hbar$  the reduced Planck's constant;  $A$ ,  $B$  and  $\omega_0$  are fitting parameters, and  $T$  is temperature, which is the independent variable. In the absence of a phase transition with increasing temperature, the phonon softening can be defined by a single theoretical curve given by Eq. (1). In the case of anomalies in the phonon softening behavior, normally a collection of curves with different fitting parameters can fit the experimental data. The point where two such adjacent curves join can be regarded as the phase transition temperature.<sup>38-40</sup> The data in Fig. 8 are modeled with two curves of Eq. (1) for each composition (solid red curves). The intersection of these two curves can be regarded as an anomaly in the  $A_1$  phonon. **For pure NBT and NBT modified with 0.5 at% and 1 at% Fe content (Fig. 8(a), (b) and (c)) an anomaly point corresponding to the expected  $T_d$  (*cf.* Table I) was determined, whereas the high experimental error prevented us from detecting any anomaly in the two Fe-rich compositions (Fig. 8(d) and (e)).**

#### IV. Discussion

Analysis of the high resolution diffraction data indicates that the room temperature structure of NBT and Fe-modified NBT is monoclinic in the  $Cc$  space group, in agreement with previous reports.<sup>6,7</sup> Although the Raman spectra measured in this work are consistent with a previous assignment of an  $R3c$  structure, this result does not exclude the presence of a monoclinic  $Cc$  phase on average. Raman spectroscopy is sensitive to the short-range crystalline order, which below  $T_d$  is dominated by the B-site polarization along the rhombohedral [111] axis. In addition, observing the higher number of Raman modes associated with a monoclinic  $Cc$  cell might prove challenging unless resonance conditions are induced.<sup>41</sup>

The piezoelectric depolarization measurements of unmodified and 1% Fe modified NBT and the high temperature XRD measurements show a transition in the same temperature range for both methods, indicating that the depolarization of NBT may be related to structural changes. The presence of a structural change is further supported by refinement of an XRD pattern of 1% Fe modified NBT at 250 °C, at which point a mixture of  $Cc$  and  $Pm\bar{3}m$  phases exists. The  $Pm\bar{3}m$  phase may describe the contribution to the diffraction pattern that results from an observation of a long-range modulated phase of  $Pnma$  platelets proposed by Dorcet *et al.*<sup>4</sup> We have previously observed similar changes with temperature in unmodified NBT.<sup>11</sup> In this prior work, the thermal depolarization of this material was correlated with an increase in the volume fraction of material which does not correlate with the long-range  $Cc$  space group.<sup>11</sup> A small inclusion of this secondary phase (2 wt%) in unmodified NBT was also observed at room temperature.<sup>11</sup> It may represent the previously reported nano-scale platelets of space group  $P4bm$  within the room temperature structure.<sup>8,9</sup> When measured using longer-range probes such as X-ray diffraction, these fractions of the

material may result in broadening of the diffraction peaks, as observed in the present work (*cf.* Fig. 3).

An inclusion of the  $Pm\bar{3}m$  phase at room temperature was also attempted in this work for the Fe-modified compositions, and a decrease in the  $Pm\bar{3}m$  phase fraction was observed with increasing Fe content. Due to the very small amount of the room temperature  $Pm\bar{3}m$  phase, a quantitative phase fraction analysis is not presented. However, possible changes in the phase fraction of this local structure may still be apparent in the diffraction data measured at room temperature as a function of Fe content. For example, the results in Figure 3 highlight an increase in definition of the 110 and 111 peak splitting with increased Fe content. Since the constituent peak positions do not shift significantly in the observed X-ray pattern, it is possible that the enhanced definition results from narrowing sample contribution to peak broadening with increased Fe substitution. This change in peak shape may be associated with a decreased contribution from a secondary phase such as  $Pm\bar{3}m$ , and is consistent with the decrease in the refined  $Pm\bar{3}m$  phase fraction for compositions with increasing Fe substitution. From this result, it is suggested that with increasing Fe substitution, the amount of this type of local disorder decreases and the structure becomes closer to the long-range  $Cc$  structure. This change also correlates with the increased distortion of the unit cell and possible increased octahedral tilting, as observed in the increasing  $a$  and  $c$  lattice parameters as well as the monoclinic  $\beta$  angle (*cf.* Table 2).

Although previous TEM studies propose the formation of an orthorhombic  $Pnma$  phase around the  $T_d$ ,<sup>4</sup> the Raman results in this work do not support the presence of such a phase in this range. Since the  $A_1$  and E bands in the 450-700  $\text{cm}^{-1}$  range will lose their LO and TO character (loss of infrared activity) upon transition to the orthorhombic structure<sup>22</sup>, it is likely that peak coalescence could be observed. In the current results, the changes seen in this wavenumber range (apparent peak coalescence, *cf.* Fig. 7(c)) cannot be associated with a

transition to such a phase. Firstly, the group-theoretical calculation for the *Pnma* phase yields  $\Gamma_{\text{Raman},Pnma}=7A_g+7B_{1g}+5B_{2g}+5B_{3g}$ ,<sup>42</sup> i.e., 24 Raman-active modes, of which some should appear for wavenumbers  $<400\text{ cm}^{-1}$ .<sup>22</sup> In the present observation, no extra modes appeared in this range. Secondly, such peak coalescence can be mimicked by other effects such as the thermal broadening of adjacent modes.

More likely, the Raman results support (in most compositions) the presence above  $T_d$  of a phase with symmetry higher than orthorhombic *Pnma*, such as tetragonal *P4bm*. The anomaly in the response of the  $A_1$  phonon at  $\sim 270\text{ cm}^{-1}$  with rising temperature can be related to changes in the Ti-O bond upon nucleation of a different phase. The presence in the lattice of nanodomains with tetragonal phase would in fact produce the local re-orientation of A-site cations along the [001] pseudo-cubic direction. This is expected to influence the strength of the Ti-O bond, thus causing in the neighborhood of  $T_d$  the anomaly in the phonon at  $\sim 270\text{ cm}^{-1}$ . The nature of the higher experimental error, which prevented us from detecting an anomaly point at  $T_d$  for the compositions with  $\text{Fe}>1.5\%$ , is not fully understood. It could be however supposed that higher Fe content (and possibly, the presence of a second phase) would increase chemical residual stress in the neighborhood of substitutional sites, thus producing local shift of the phonon line center. Since for each temperature a different point of the specimen surface is observed, this could explain the observed error. The changes in the  $A_1$  phonon are detected at lower temperatures than measured by *ex situ* depolarization. This is probably due to Raman spectra being sensitive to changes in the short range order. Our experiments cannot discriminate an antiferroelectric character of the nanodomain phase, since only wavenumbers  $>\sim 150\text{ cm}^{-1}$  can be examined with the current setting. Access to A-site modes would provide information on possible antiparallel cation-ion displacements in the *P4bm* phase, leading to antiferroelectric properties. Further temperature-dependent

Raman experiments in this wavenumber range using different excitation wavelengths (i.e., to induce resonance) may be insightful.

Depolarization measurements indicate that the addition of 0.5 and 1 at% Fe to NBT increases the piezoelectric depolarization temperature, while further increase in Fe content then leads to a decrease in  $T_d$ . The initial increase in  $T_d$  with small amounts of Fe is confirmed by both Raman and XRD and may be due to defect dipoles which form with the addition of Fe to NBT.<sup>43</sup> The presence of such defect dipoles can stabilize ferroelectric order in the material and therefore increase the  $T_d$ .<sup>44</sup> The subsequent decrease in  $T_d$  due to higher Fe substitution may be associated with limited ferroelectric poling due to the high conductivity of these samples. The transitions observed in Raman and XRD measurements near the piezoelectric depolarization temperature indicate that a structural change occurs at this temperature. A similar increase then subsequent decrease in  $T_d$  was also reported for doping with  $Ba^{2+}$  by Hiruma<sup>10</sup> and Cordero<sup>45</sup>. This change in  $T_d$  with  $Ba^{2+}$  doping implies that the same structural changes may be taking place in Ba-modified NBT as in Fe-modified NBT.

It was observed in Fig. 1 that with the addition of 0.5 at% Fe the room temperature  $d_{33}$  remains the same as in unmodified NBT. However, further Fe addition to the system leads to a decrease in the room temperature  $d_{33}$  value. This result is quite different from what is found in PZT. Rema *et al.* reported that with the addition of 0.5 at% Fe to a PZT based material, the  $d_{33}$  dropped significantly from approximately 370 to 250 pC/N at room temperature.<sup>46</sup> The decrease in both the room temperature  $d_{33}$  and the  $T_d$  which is observed at higher levels of Fe substitution may be associated with limited substitution of Fe in this material. Although the diffraction patterns of these materials only indicated the presence of a second phase in the 2 at% Fe composition, previous work using electron paramagnetic resonance showed that a second phase forms in concentrations as low as 1.5 at% Fe.<sup>43</sup> This

second phase could lead to the increased conductivity in the compositions with higher Fe, limiting the ferroelectric poling process. It is also likely that the increase in lattice parameters between unmodified and 1.5 at% Fe has resulted in significant lattice strain. A further increase in Fe-modification beyond 1.5 at% has led to the formation of a second phase in order to decrease the lattice strain. This is an important observation for future application of these materials, as the solubility limit in PZT is higher than what was found in this study for NBT.

## V. Conclusions

The crystal structure of unmodified and Fe-modified NBT was examined as a function of increasing Fe content, and with increasing temperature. The piezoelectric properties were also examined as a function of temperature in order to understand the impact of Fe on piezoelectric depolarization. The addition of Fe to NBT did not change the phase of the material, however with low Fe addition (i.e., 0.5 and 1.0 at%) it led to an increase in the  $T_d$  followed by a slight decrease with higher Fe content. This temperature dependence in the electrical properties as a function of Fe composition was mirrored in the structural studies using XRD and Raman spectroscopy. An analysis of the XRD data as a function of temperature indicated that there is a portion of the diffraction pattern at elevated temperatures which cannot be fully described using the  $Cc$  model. This portion is attributed to a growth in the volume fraction of nano-scale regions, modeled in this work as a  $Pm\bar{3}m$  phase. An anomaly in the  $A_1$  phonon assigned to Ti-O vibrations was found to correlate well with  $T_d$  in most compositions, thus implying that a structural transition exists on the short range at a temperature near the piezoelectric depolarization, and that the temperature of this transition shifts with Fe addition. The analysis of the XRD patterns and the Raman spectra as a function of temperature supports the view that the process of piezoelectric depolarization in

NBT-based materials occurs due to the formation of nano-scale regions which disrupt the long-range ferroelectric order rather than a long-range phase transition.

### **Acknowledgements**

EA and JJ acknowledge partial support for this work by the U. S. National Science Foundation (NSF) under award numbers DMR-0746902 and OISE-0755170. JF, BK, and JJ acknowledge support from the U.S. Department of the Army under W911NF-09-1-0435. Use of the Advanced Photon Source (APS) was supported by the U. S. Department of Energy, Office of Science, Office of Basic Energy Sciences, under Contract No. DE-AC02-06CH11357. MD gratefully acknowledges financial support by the Austrian Federal Government (in particular from the Bundesministerium für Verkehr, Innovation und Technologie and the Bundesministerium für Wirtschaft und Arbeit) and the Styrian Provincial Government, represented by Österreichische Forschungsförderungsgesellschaft mbH and by Steirische Wirtschaftsförderungsgesellschaft mbH, within the research activities of the K2 Competence Centre on “Integrated Research in Materials, Processing and Product Engineering”, operated by the Materials Center Leoben Forschung GmbH in the framework of the Austrian COMET Competence Centre Programme. DD acknowledges support of SNSF PNR62 project No. 406240\_126091. The authors acknowledge the help of Dr. Matthew Suhomel (measurements at the APS) and Prof. Ronald J. Bakker (measurements at the Montanuniversitaet Leoben).

## References

- 1 G. Smolenskii, V. Isupov, A. Agranovskaya, and N. Krainik, Soviet Physics-Solid State **2**, 2651 (1961).
- 2 G. O. Jones and P. A. Thomas, Acta Crystallographica Section B-Structural Science **58**, 168 (2002).
- 3 I. P. Pronin, P. P. Syrnikov, V. A. Isupov, V. M. Egorov, and N. V. Zaitseva, Ferroelectrics **25**, 395 (1980).
- 4 V. Dorcet, G. Trolliard, and P. Boullay, Chemistry of Materials **20**, 5061 (2008).
- 5 G. Trolliard and V. Dorcet, Chemistry of Materials **20**, 5074 (2008).
- 6 S. Gorfman and P. A. Thomas, Journal of Applied Crystallography **43**, 1409 (2010).
- 7 E. Aksel, J. Forrester, J. Jones, P. Thomas, K. Page, and M. Suchomel, Applied Physics Letters **98** (2011).
- 8 V. Dorcet and G. Trolliard, Acta Materialia **56**, 1753 (2008).
- 9 R. Beanland and P. A. Thomas, Scripta Materialia **65**, 440 (2011).
- 10 Y. Hiruma, H. Nagata, and T. Takenaka, Journal of Applied Physics **105**, 084112 (2009).
- 11 E. Aksel, J. S. Forrester, B. Kowalski, J. L. Jones, and P. A. Thomas, Applied Physics Letters **99**, 222901 (2011).
- 12 Y. Watanabe, Y. Hiruma, H. Nagata, and T. Takenaka, Ferroelectrics **358**, 139 (2007).
- 13 M. Davies, E. Aksel, and J. Jones, Journal of the American Ceramic Society **94**, 1314 (2011).
- 14 Y. Hiruma, K. Yoshii, R. Aoyagi, H. Nagata, and T. Takenaka, Key Engineering Materials **320**, 23 (2006).
- 15 B. Wylie-van Eerd, D. Damjanovic, N. Klein, N. Setter, and J. Trodahl, Physical Review B **82**, 104112 (2010).
- 16 A. Slodczyk, P. Daniel, and A. Kania, Physical Review B **77**, 184114 (2008).
- 17 A. Slodczyk and P. Colomban, Materials **3**, 5007 (2010).
- 18 A. Feteira, D. C. Sinclair, and J. Kreisel, Journal of the American Ceramic Society **93**, 4174 (2010).
- 19 M. Deluca, H. Fukumura, N. Tonari, C. Capiani, N. Hasuike, K. Kisoda, C. Galassi, and H. Harima, Journal of Raman Spectroscopy **42**, 488 (2011).
- 20 M.-S. Zhang, J. F. Scott, and J. A. Zvirgzds, Ferroelectrics Letters Section **6**, 147 (1986).
- 21 J. Kreisel, A. M. Glazer, G. Jones, P. A. Thomas, L. Abello, and G. Lucazeau, Journal of Physics: Condensed Matter **12**, 3267 (2000).
- 22 J. Kreisel, A. Glazer, P. Bouvier, and G. Lucazeau, Physical Review B **63**17, 174106 (2001).
- 23 J. Petzelt, et al., Journal of Physics-Condensed Matter **16**, 2719 (2004).
- 24 D. Rout, K.-S. Moon, S.-J. L. Kang, and I. W. Kim, Journal of Applied Physics **108**, 084102 (2010).
- 25 L. Luo, W. Ge, J. Li, D. Viehland, C. Farley, R. Bodnar, Q. Zhang, and H. Luo, Journal of Applied Physics **109** (2011).
- 26 D. Berlincourt, The Journal of the Acoustical Society of America **91**, 3034 (1992).
- 27 X. L. Zhang, Z. X. Chen, L. E. Cross, and W. A. Schulze, Journal of Materials Science **18**, 968 (1983).
- 28 H. Nagata and T. Takenaka, in *Applications of Ferroelectrics, 2000. ISAF 2000. Proceedings of the 2000 12th IEEE International Symposium on*, 2000), p. 45.

- 29 A. Watcharapasorn, S. Jiansirisomboon, and T. Tunkasiri, *Materials Letters* **61**, 2986  
(2007).
- 30 A. C. Larson and R. B. Von Dreele, General Structure Analysis System (GSAS), Los  
Alamos National Laboratory Report LAUR, 86 (2000).
- 31 P. Stephens, *Journal of Applied Crystallography* **32**, 281 (1999).
- 32 J. E. Daniels, J. L. Jones, and T. R. Finlayson, *Journal of Physics D: Applied Physics*  
**39**, 5294 (2006).
- 33 C. Ma, X. Tan, E. Dul'kin, and M. Roth, *Journal of Applied Physics* **108**, 104105  
(2010).
- 34 J. E. Daniels, W. Jo, J. Rodel, D. Rytz, and W. Donner, *Applied Physics Letters* **98**,  
252904 (2011).
- 35 A. Reyes, C. de la Vega, M. E. Fuentes, and L. Fuentes, *Journal of the European  
Ceramic Society* **27**, 3709 (2007).
- 36 H. Fukumura, H. Harima, K. Kisoda, M. Tamada, Y. Noguchi, and M. Miyayama,  
*Journal of Magnetism and Magnetic Materials* **310**, e367 (2007).
- 37 M. Balkanski, R. F. Wallis, and E. Haro, *Physical Review B* **28**, 1928 (1983).
- 38 A. P. Litvinchuk, M. N. Iliev, V. N. Popov, and M. M. Gospodinov, *Journal of  
Physics: Condensed Matter* **16**, 809 (2004).
- 39 H. Fukumura, S. Matsui, H. Harima, K. Kisoda, T. Takahashi, T. Yoshimura, and N.  
Fujimura, *Journal of Physics: Condensed Matter* **19**, 365239 (2007).
- 40 H. Fukumura, N. Hasuike, H. Harima, K. Kisoda, K. Fukae, T. Takahashi, T.  
Yoshimura, and N. Fujimura, *Journal of Physics: Conference Series* **92**, 012126  
(2007).
- 41 J. Rouquette, J. Haines, V. Bornand, M. Pintard, P. Papet, and J. L. Sauvajol, *Physical  
Review B* **73**, 224118 (2006).
- 42 P. Gillet, F. Guyot, G. D. Price, B. Tournier, and A. Cleach, *Physics and Chemistry  
of Minerals* **20**, 159 (1993).
- 43 E. Aksel, E. Erdem, P. Jakes, J. Jones, and R. Eichel, *Applied Physics Letters* **97**  
(2010).
- 44 W. Jo, E. Erdem, R.-A. Eichel, J. Glaum, T. Granzow, D. Damjanovic, and J. Rodel,  
*Journal of Applied Physics* **108**, 014110 (2010).
- 45 F. Cordero, F. Craciun, F. Trequattrini, E. Mercadelli, and C. Galassi, *Physical  
Review B* **81** (2010).
- 46 K. Rema, V. Etacheri, and V. Kumar, *Journal of Materials Science: Materials in  
Electronics* **21**, 1149 (2010).

## Figure Captions

FIG. 1. (Color Online) Longitudinal piezoelectric coefficient  $d_{33}$  measured as a function of temperature for various compositions of Fe-modified NBT. The converse  $d_{33}$  was measured *in situ* (a) and the direct  $d_{33}$  was measured *ex situ* (b).

FIG. 2. (Color Online) Permittivity and loss measured as a function of temperature at 0.1, 1, 10, 100, and 1000 kHz for (a) unmodified NBT poled, (b) unmodified NBT unpoled, (c) 0.5 at% Fe modified poled, and (d) 0.5 at% Fe modified unpoled.

FIG. 3. (Color Online) Excerpts of high resolution XRD patterns of NBT with varying Fe concentrations. For simplicity, peaks are labeled relative to the pseudocubic planes.

FIG. 4. (Color Online) Rietveld refinement of a high resolution XRD pattern of 1% Fe-modified NBT showing the observed pattern (x) and the calculated fit (—). The line below is the difference between the observed and calculated intensities.

FIG. 5. (Color Online) Excerpts of high resolution XRD patterns of 1% Fe-modified NBT at various temperatures.

FIG. 6. (Color Online) Selected areas of XRD patterns of (a) unmodified and (b) 1% Fe modified NBT plotted as a function of temperature.

FIG. 7. (Color Online) (a) Raman spectrum of unmodified NBT at room temperature.

Spectral deconvolution was performed according to eight Gaussian-Lorentzian modes based on literature.<sup>20, 21</sup> The assignment of spectral modes to specific vibrations in the crystal lattice is superimposed on the graph. (b) Raman spectra of unmodified and modified NBT at room temperature. **The spectral signature is not greatly affected by Fe-modification.** (c) Raman spectra of unmodified NBT as a function of temperature. The displayed temperatures refer to the setting of the heating stage at 20 °C steps. **The**

apparent peak coalescence in the mid-frequency region can be ascribed to intrinsic thermal broadening.

FIG. 8. (Color Online) Variation of  $A_1$  phonon line center ( $\sim 270 \text{ cm}^{-1}$ ) as a function of temperature for all compositions: (a) unmodified NBT, (b) NBT with 0.5 at% Fe, (c) NBT with 1 at% Fe, (d) NBT with 1.5 at% Fe, and (e) NBT with 2 at% Fe. Intersection (anomaly) points between two fitting datasets (red line) are highlighted by continued dashed lines, and are observed only in compositions up to 1 at% Fe. The detected anomaly points can be associated with changes in the short-range structure occurring at  $T_d$ . For higher Fe content the higher experimental error prevents from detecting any anomaly point, and thus fitting in (d) and (e) is presented considering the  $T_d$  values obtained from the depolarization study as first approximation.

**Table I** - Depolarization temperatures,  $T_d$  (°C), as measured by Raman spectroscopy, *in situ* converse  $d_{33}$ , *ex situ* direct  $d_{33}$  and synchrotron XRD in all investigated compositions.

Uncertainty in  $T_d$  determination by Raman is  $\pm 10$  °C.

Composition	Raman spectroscopy	Converse $d_{33}$ ( <i>in situ</i> )	Direct $d_{33}$ ( <i>ex situ</i> )	Permittivity	Synchrotron XRD
Unmodified	161	161	210	176	195
0.5% Fe	201	191	233	202	-
1% Fe	181	190	219	-	220
1.5% Fe	-	175	199	-	-
2% Fe	-	177	201	-	-

**Table II** - Refined lattice parameters and Bragg fitting values for the samples with increasing Fe-modification.

at% Fe in NBT <i>Cc</i> setting	a (Å)	b (Å)	c (Å)	$\beta$ (°)	Cell Volume (Å <sup>3</sup> )	Fitting Values
0	9.5255(2)	5.48262(4)	5.50751(5)	125.3467(5)	234.609(5)	$R_p$ 5.30% $R_{wp}$ 7.36% $\chi^2$ 4.03
0.5	9.5284(2)	5.48260(3)	5.51027(3)	125.3598(6)	234.760(5)	$R_p$ 5.58% $R_{wp}$ 7.88% $\chi^2$ 4.54
1.0	9.5310(2)	5.48260(4)	5.51112(5)	125.3632(5)	234.845(5)	$R_p$ 5.54% $R_{wp}$ 7.62% $\chi^2$ 3.23
1.5	9.5322(2)	5.48263(4)	5.51263(5)	125.3775(5)	234.902(5)	$R_p$ 5.75% $R_{wp}$ 8.04% $\chi^2$ 3.01
2.0*	9.5322(2)	5.48454(5)	5.51327(6)	125.3785(9)	235.007(7)	$R_p$ 5.02% $R_{wp}$ 7.07% $\chi^2$ 3.50

\*This refinement includes the addition of BFO as a second phase.

**Table III** - Refined lattice parameters and Bragg fitting values for 1 at% Fe-modified NBT with increasing temperature.

Temp. (°C)	Space Group	a (Å)	b (Å)	c (Å)	$\beta$ (°)	Fitting Values
30	<i>Cc</i>	9.5310(2)	5.48260(4)	5.51112(5)	125.3632(5)	$R_p$ 5.54% $R_{wp}$ 7.62% $\chi^2$ 3.23
100	<i>Cc</i>	9.5300(1)	5.48838(2)	5.51071(3)	125.3310(3)	$R_p$ 4.98% $R_{wp}$ 6.67% $\chi^2$ 2.466
250	<i>Cc</i> (15%)	9.54071(9)	5.50099(3)	5.51627(5)	125.2817(8)	$R_p$ 4.66% $R_{wp}$ 6.09% $\chi^2$ 2.078
	<i>Pm</i> $\bar{3}$ <i>m</i> (85%)	3.894524(4)				
300	<i>P4bm</i>	5.508967(4)	5.508967(4)	3.901071(4)		$R_p$ 4.87% $R_{wp}$ 6.63% $\chi^2$ 2.474
400	<i>P4bm</i>	5.515873(3)	5.515873(3)	3.907307(4)		$R_p$ 4.64% $R_{wp}$ 6.33% $\chi^2$ 2.245
600	<i>Pm</i> $\bar{3}$ <i>m</i>	3.912961(5)	3.912961(5)	3.912961(5)		$R_p$ 5.04% $R_{wp}$ 7.28% $\chi^2$ 2.931

Figure 1

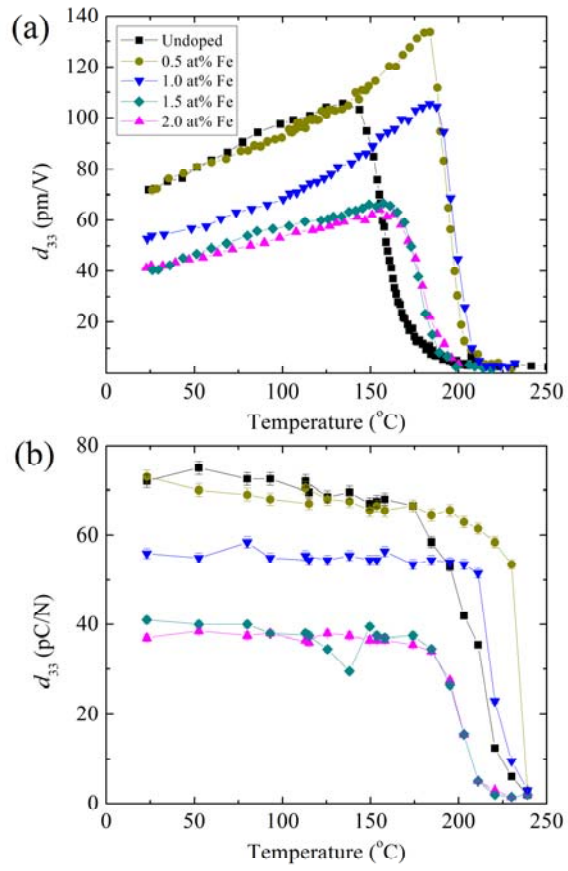


Figure 2

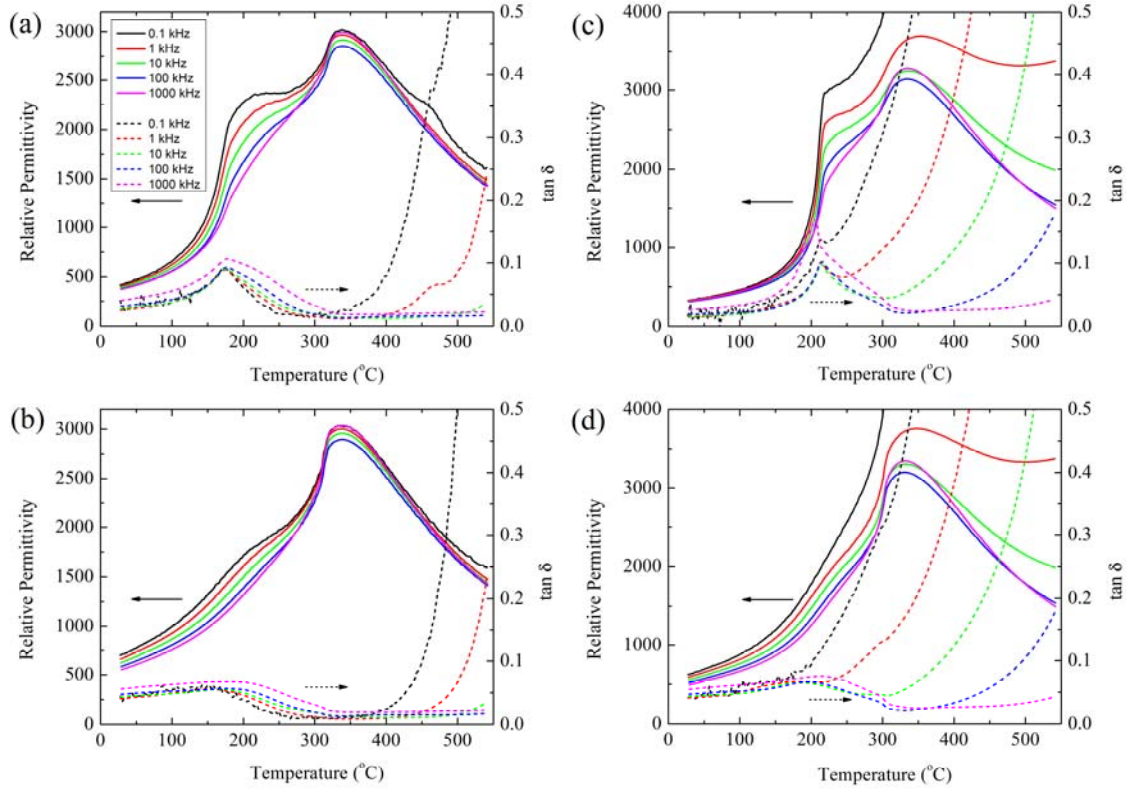


Figure 3

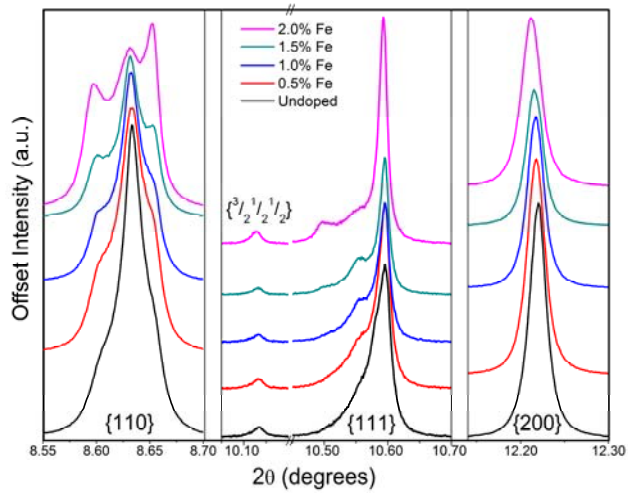


Figure 4

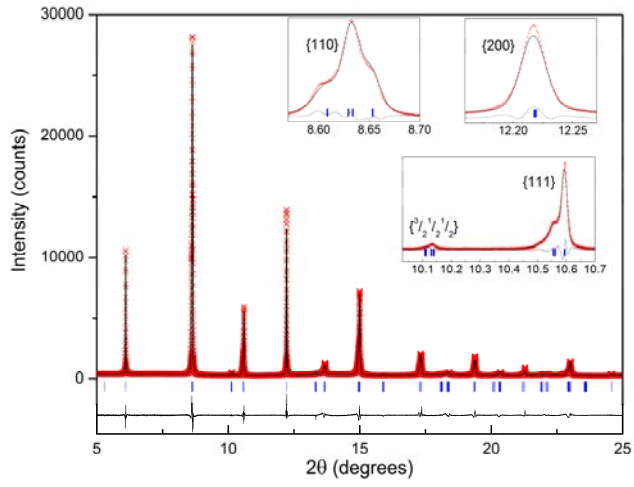


Figure 5

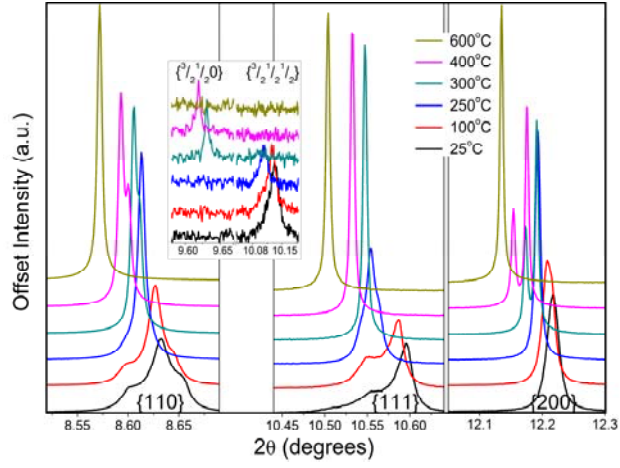


Figure 6

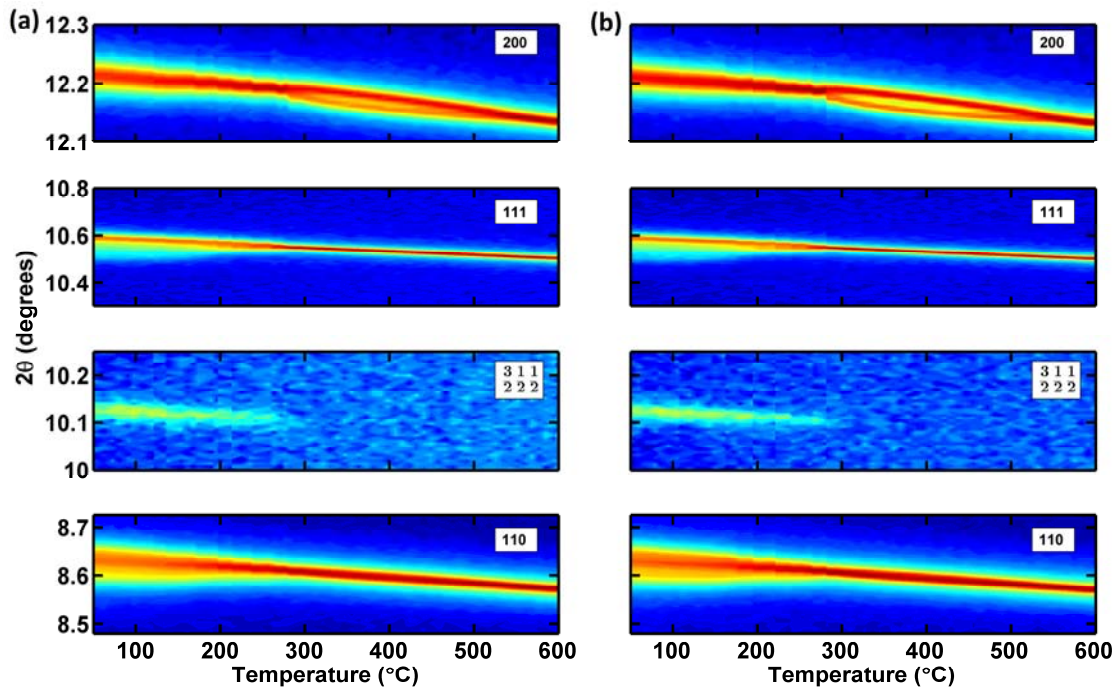


Figure 7

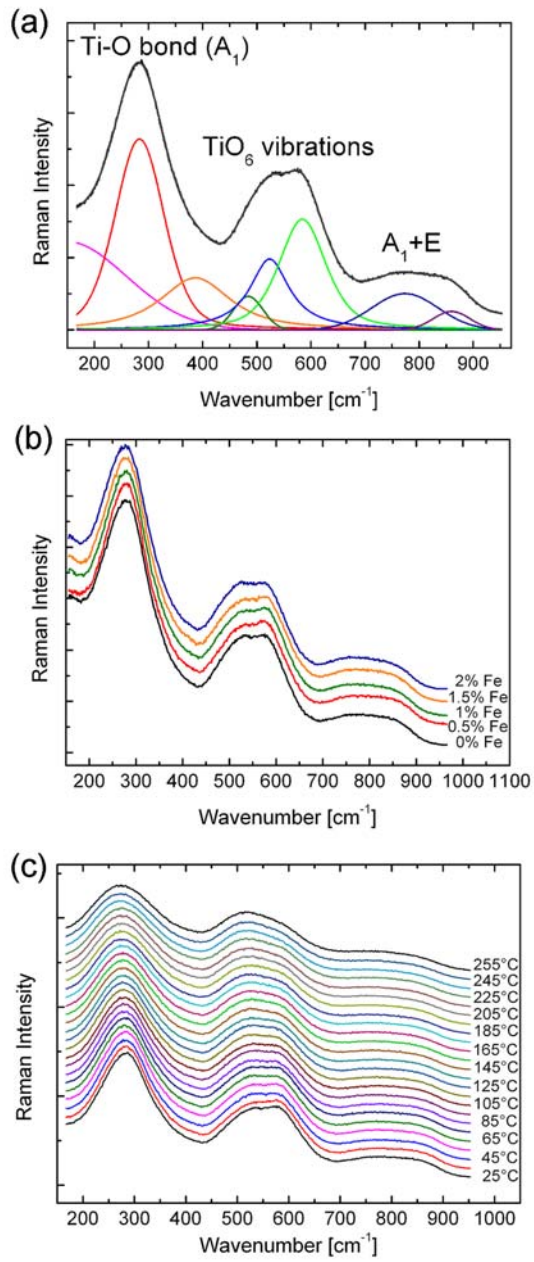


Figure 8

